Supplement of Atmos. Chem. Phys., 21, 18175–18194, 2021
https://doi.org/10.5194/acp-21-18175-2021-supplement

Atmospheric Chemistry and Physics
Open Access
EGU

Supplement of

Measurement report: Characterization of uncertainties in fluxes and fuel sulfur content from ship emissions in the Baltic Sea

Jari Walden et al.

Correspondence to: Jari Walden (jari.a.walden@gmail.com)

Uncertainty estimates of the fluxes

The uncertainty estimates of the results for the fluxes measured by the gradient technique and for the FSC are presented in more detail here. Following the procedure by JCGM (JCGM 2008), each of the uncertainty sources in the measurement system that contributes to the dispersion of the measurement results needs to be characterized. In case of the gradient technique, the flux is described by Eq. (5), and the uncertainty of the measurement result is described by Eq. (11). Single standard uncertainties that are considered to contribute to the uncertainty of the flux measurement result are the friction velocity u^*, the integral of the dimensionless potential function Ψ_c, the measurement height z, and the uncertainty of the measured concentrations of gases and particles. A more detailed description of the sources of errors is found in the literature (Businger, 1986). Of additional sources, nonstationarity, was only partly considered here, whereas errors that flow distortion introduces in the measurement height and the wind speed were corrected. On the other hand, the chemically reactive species NO, O_3, and NO_2 were not considered in detail since the concentration difference between the two measurement heights did not exceed the uncertainty limit calculated for these compounds (Fig. S2). Eq. (11) was applied to each of the uncertainty sources in Eq. (5), resulting in an equation that includes a weighting factor and the standard uncertainty of each of the uncertainty sources. The weighing factors were calculated from the measurement results, and each of the uncertainty sources were estimated by the standard deviation of the results or by other means, e.g. by the performance characteristics of the measurement instrument (analyzers etc.). Uncertainties of the analyzers for gaseous compounds and particles were based on the performance characteristics of the analyzers themselves. In case of the analyzers that measure the concentration of ozone, nitrogen oxides and sulfur dioxide, (APOA-370 2006, Environnemet AC31M 2006, Thermo 43i 2006) a complete test report showing the performance characteristics that influence the measurement results has been prepared and made available by the Immissionsschutz und Energiesysteme GmbH, TÜV, (www.qal1.de). Modifications in the complete procedure defined by TÜV were made to fit for the purpose of the measurements conducted at Harmaja. Concerning the CO_2 measurements, the performance of the Licor 7000 and Picarro G2301 analyzers were obtained from the document of the WMO/GAW guidelines (WMO 2013). In case of the particle measurements, the performance of the two ELPI instruments, i.e. ELPI1 and ELPI2, was tested during the measurements. After the HEPA filtration tests and zero setting the same air sample was injected into both instruments at certain time frames and at different particle concentrations. The effective variance regression line between the two ELPI instruments (assuming that both instruments have the same statistical uncertainty) was used to correct the results of the ELPI2 with respect to the ELPI1. The correction coefficients were inferred for the 8 smallest stages of the ELPI2 (dN/dlogDp), and for the number concentration of particles smaller than 1 μm (Ntot). Only the Ntot concentrations (not the size distributions) from ELPI2 were used in this study. The standard and expanded uncertainties of the instruments with respect to each other was then inferred from the scatter of the Ntot results from the ELPIs (Figs. 1h and 2h). All measured Ntot data from the ELPI2 were corrected accordingly. This strategy was different from that of the gaseous compounds, for which actual uncertainties of the analyzer results have been obtained. In Fig. S1, the expanded uncertainty of each analyzer is presented as a function of concentration. The differences in the concentrations of the gaseous compounds and number concentrations of nanoparticles from the measurement heights are presented in Fig. S2 together with the uncertainty of the analyzers. Once the difference of the concentrations exceeds the uncertainty limit, the difference is acceptable; otherwise, there is no detectable concentration difference and these measurement results were eliminated. All the uncertainty sources for the flux measurements by the gradient technique are presented in Table S1. The contribution of the friction velocity is obtained from the uncertainty analysis for the EC method since it was taken from the sonic measurements. Two meteorological situations were included: stationary and prevailing situations over the measurement period. The prevailing meteorological situations gives a major contribution to the uncertainty budget while contribution of stationary meteorology is not large.

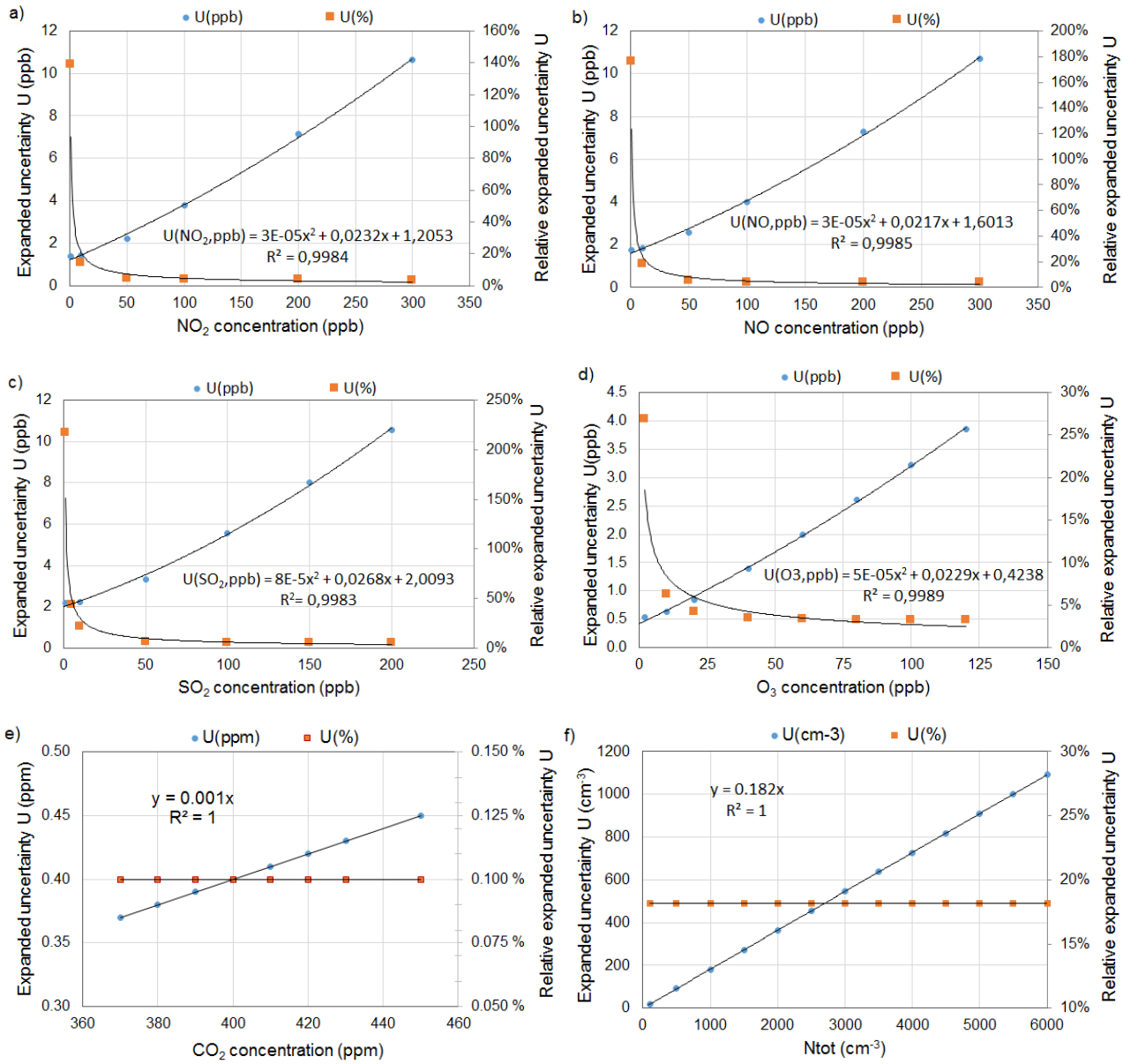

Figure S1. Expanded uncertainties of the measurement results for gaseous compounds and particle number concentration. Figures 2a to 2e represents NO_2-, NO-, SO_2-, O_3- and CO_2-measurements while 2f represents relationship between two particle measurement instrument with standard error of the estimate ($\sigma = 493$).

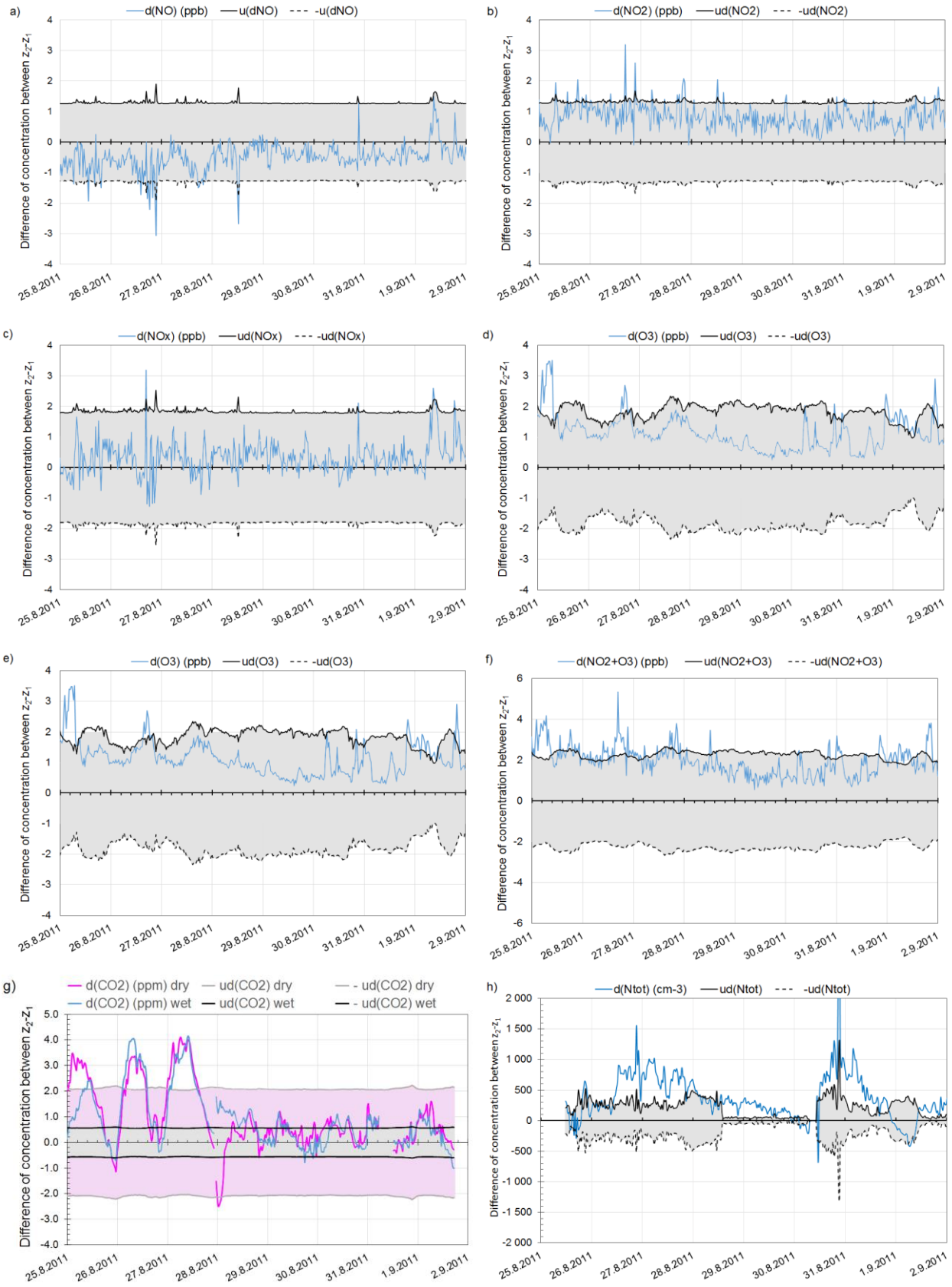

Figure S2. Time series of the 30 min averaged concentration differences between the measurement heights for gaseous compounds (a-g) and number concentration of nanoparticles (h) during the measurement campaign in 2011. CO_2 concentrations in (g) are wet and dry concentrations. Also shown are the standard uncertainties of the analyzers (curves showing $\pm u_d$). Note that the expanded uncertainties of the analyzers (U) shown in Fig. S1 are doubles of the standard uncertainties. The concentration differences within the uncertainty curves (shaded areas) were not used for the flux calculations.Consequently, the fluxes were calculated only for Ntot.

Table S1. Estimated relative standard uncertainties u (%) for each of the contributing sources (eq. 12 in the text). as well as the relative expanded uncertainty of the fluxes U (%) are presented (see in the text). The fluxes were calculated by the GR method. Sub index 1 refers to the lower and index 2 to the higher measurement height, and S refers to the median concentation over the measurement period. The relative expanded uncertainty is presented in situations of stationary meteorology ($U_{Stat.Met}$) during the measurement campaigns for Ntot. For the gases the fluxes were not clearly detectable (Fig. S2).

Uncertainty source	Uncertainty source	Standard uncertainty, u			single uncertainties and parameters		Weight $(\partial F(x_i)/\partial x_i)^2$	Standard uncertainty, *u(%)*
Flux of gases and particles	$Fc = -\frac{ku_*(c(z_2)-c(z_1))}{\left(\ln\left(\frac{z2}{z_1}\right)-\Psi_c(\zeta 2)+\Psi_c(\zeta 1)\right)}$	$\frac{u_c(F_c)^2}{F_c^2}=\frac{u(u_*)^2}{u_*^2}+\frac{u(\Psi_h)^2}{\left(\ln\left(\frac{z_2}{z_1}\right)-\Delta\Psi_h\right)^2}+\frac{u(\Delta c)^2}{\Delta c^2}+\frac{u(z)^2}{\left(\ln\left(\frac{z_2}{z_1}\right)-\Delta\Psi_h\right)^2}\left(\frac{1}{z_1^2}+\frac{1}{z_2^2}\right)+u(ws)^2$						
Friction velocity	$u_* = \left(\overline{-u'w'}\right)^{1/2}$	stationary meteorology, see in text					1.000	**7.0 %**
Integral function, Ψh	$\Psi h = \int_{\zeta_0}^{\zeta}(1-\phi_h(\zeta'))d\zeta'/\zeta']$	$\left(\frac{u(\Delta\Psi)}{\Delta\Psi}\right)^2=\frac{u(\varphi)^2}{(1-\varphi)\hat{}2}+[(\frac{1}{\zeta 1})^2+(\frac{1}{\zeta 2})^2]\cdot(\frac{u(\zeta)}{\ln(\frac{z_2}{z_1})})^2$			$u(\varphi_h)$ $\varphi_{h,ave}$ $u(\varphi_h,\%)$ $\Delta\Psi$	0.10 0.56 17.1 % -0.0747	0.222	**26.4 %**
	$\Delta\Psi=(1-\varphi_{h(ave)})\ln(\zeta_2/\zeta_1)$							
Stability parameter ζ								
	ζ_1				$u(\zeta_{z1})$ $\zeta_{z1,ave}$	0.06 -0.07		
	ζ_3				$u(\zeta_{z2})$ $\zeta_{z2,ave}$	0.07 -0.08		
Measurement height, m	Concentration C_2 at Z_2 Concentration C_1 at Z_1	$(z_1^2+z_2^2)/[z_1{*}z_2{*}\ln(z_2/z_1)\text{-}\Delta\Psi)]^{2*}u(z)^2$			z_1(m) z_2(m) u_{zm}(cm) u_{zr}(cm)	7.2 10.7 **50.0** **75.0**	0.126	8.4 %
Concentration, C			$u(S_{zi})$	$u(S_{zi}())$	$u(S_z())$	$u(\Delta S_z(\%)$	S_{z1}(c/cm^3)	S_{z2}(c/cm^3)
	Particles, Ntot	$\left(\frac{u(\Delta S)}{\Delta S}\right)^2=\|(u(S_{,2})^2+(u(S_1)^2\|^2$	$u(N_{tot,z2})$	272.30	341.78	**9.10 %**	3755	4951
			$u(N_{tot,z1})$	206.55				
Wind speed, WS	**Correction of wind speed with CFD calculation**		$u(ws(z))$				1	8.90 %
Expanded uncertainty of flux				**Flux(median)**		**$U(\%)_{Stat.Met}$**		
	$U(F_{Ntot})$%			**-229.1**		**30.8 %**		

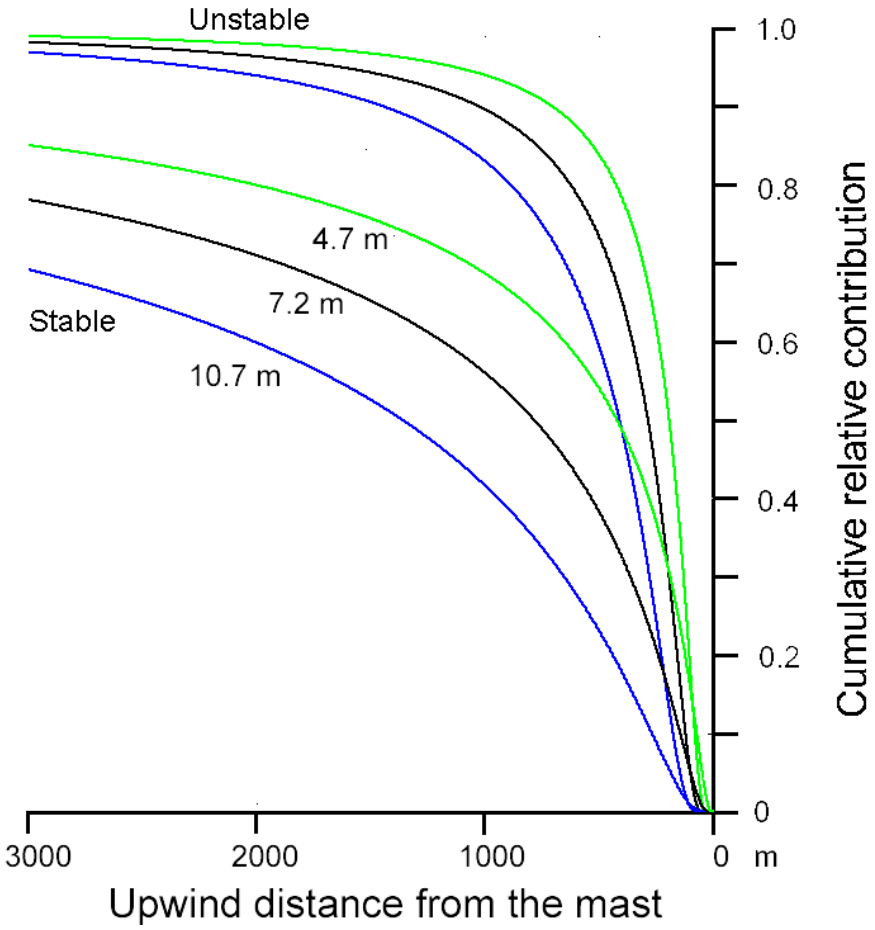

Figure S3. Cumulative relative contribution of flux footprint area as a function of upwind distance from the mast at stable and unstable stratification (L= + 100 m and L = -100 m). The CO_2 instruments located at the altitudes of 10.7 m and 7.2 m, and the ELPIs at 7.2 m and 4.7 m, as recalculated in Fig. 3a.

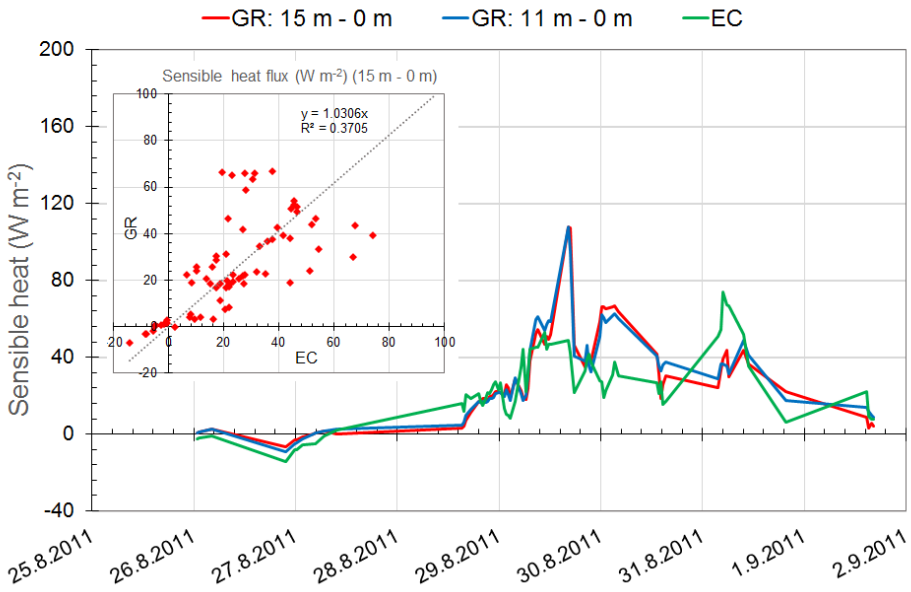

Figure S4. Sensible heat by the GR and EC methods at Harmaja 2011. The scatter figure between the two methods is shown in the small figure.

Figure S5 shows the WPL correction for water vapor with respect to uncorrected CO_2 flux in the campaigns at Harmaja 2011 and Harmaja 2012. Correction for temperature was omitted as described in the text (p. 15, line 441-442). As can be seen, during the period of 28.8 to 31.8 the WPL correction for water vapor was significant changing even the sign of the CO2 flux. At Harmaja 2012 the influence of the WPL correction was clearly less than in the campaign in 2011. In the attached figure the period when the air masses were arriving from the Atlantic Ocean, i.e. 28.8. to 31.8., the latent heat flux increased 3 to 6 times compared to the rest of the period thus explaining the change of the sign of the CO_2 flux.

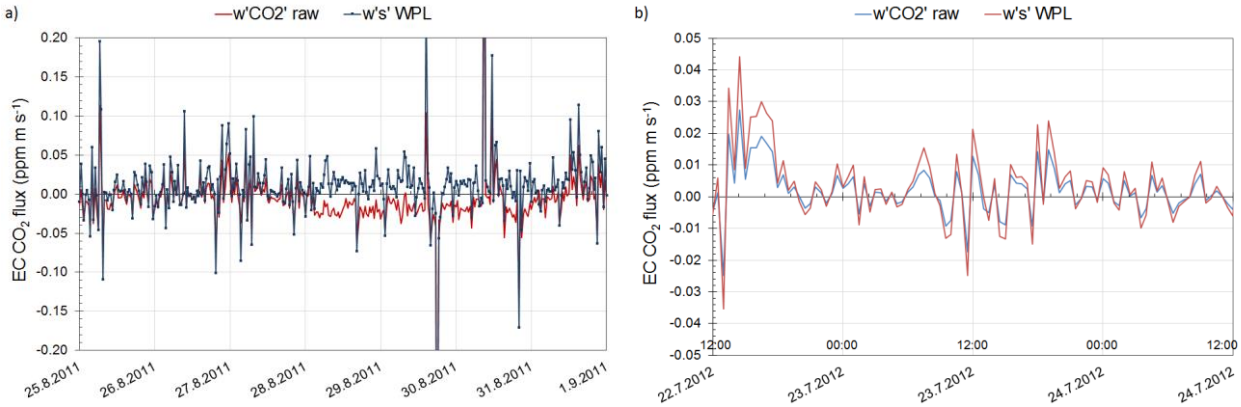

Figure S5. Comparison of the raw CO_2 flux (w´CO2´ raw) and the WPL correction (w´s´ WPL) at Harmaja in 2011 (a) and 2012 (b).

Figure S6 shows the differences on the time averages and respond times during the Harmaja measurement campaign in 2012. In Fig. S6a the time series of the ΔSO_2 and ΔCO_2 concentrations are presented at two different time integration: 15 s and 1 min. The response time of the SO_2 analyzer, Thermo 34 CTL, was improved to 15 s by changing the sample flow rate and shortening the sample tubes inside the analyser. The respond time of the CO_2 analyzer, Picarro G2301, was less than 1s. The calculated FSCs were nearly the same for both cases when the results were obtained from the peak areas. However, the FSC calculated from the peak area value was somewhat higher compared to that of the peak maximum value, in this case 0.46% and 0.40%, respectively. In Fig. S6b the emission peak of CO_2 is illustrated at three different time integration: 1 sec, 15 sec and 1 minute resulting peak area as 34.1 ppm min, 33.25 ppm min, and 33.14 ppm min, respectively. The response time of the analyser defines the shortest integration time of the data collection.

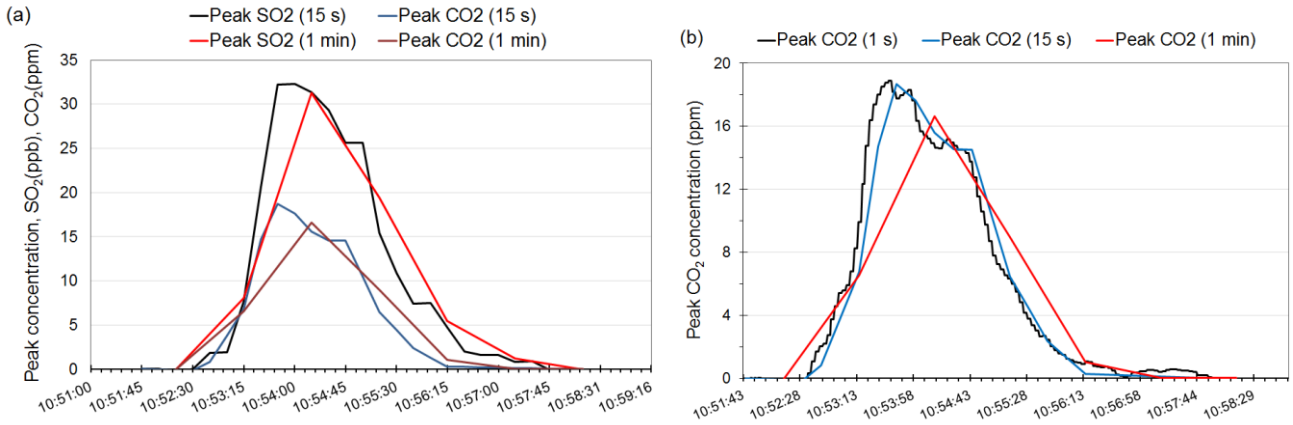

Figure S6. Comparison of the ship emission peak with different time frequency of data collection and response time for SO_2 and CO_2 (a) and CO_2 peak with different time averages (b). Background concentrations were subtracted.